Impact of Horizontal Resolution on the Numerical Simulation of a Midlatitude Squall Line: Implicit versus Explicit Condensation

STÉPHANE BÉLAIR AND JOCELYN MAILHOT

Meteorological Research Branch, Meteorological Service of Canada, Dorval, Quebec, Canada

(Manuscript received 19 June 2000, in final form 5 March 2001)

ABSTRACT

The relative roles of implicit and explicit condensation schemes in the numerical representation of a squall line that occurred on 7–8 May 1995 over the southern Great Plains are examined in this study using Mesoscale Compressible Community model integrations at 2-, 6-, 18-, and 50-km resolution. Results from the 2-km model in which condensation is explicitly represented agree best with observations and are used as ''synthetic'' data to evaluate the performance of lower-resolution configurations.

It is found that the representation of the squall system greatly deteriorates as resolution is decreased and that the relative roles of the implicit and explicit condensation schemes change dramatically. At 6-km resolution, the leading convective band is barely resolved by the model, and the implicit–explicit partition of precipitation is ambiguous because both implicit and explicit schemes are active simultaneously at the leading edge of the system. In spite of this ambiguity, it is found that use of a deep convection scheme is still beneficial to the squall-line simulation. At 18 km, the convective line is not resolved by the model, and its effect is completely due to the implicit scheme. The mesoscale circulations in the trailing anvil region of the squall system are generated at the small end of the model resolvable scales and are exaggeratedly intense. There is no ambiguity concerning the partition of condensation into implicit and explicit components at this resolution, but the relative intensity of precipitation produced by the two cloud schemes is opposite to what is observed, considering that the implicit scheme is supposed to represent subgrid-scale convection at the leading edge of the system, and the explicit scheme the grid-scale condensation in the trailing anvil. At 50 km, both the leading convection and the mesoscale circulations in the trailing anvil have to be parameterized because they are not resolved at the model grid scale. The precipitation and internal structures associated with the squall line are thus not well represented at this resolution.

The results also show that all the configurations produce precipitation accumulations that are much larger than observations. This problem is most important at 18-km resolution. Grid-scale condensation is mostly responsible for this rainfall overestimation. It is suggested that this problem is linked to a misrepresentation of convective-scale processes.

1. Introduction

Precipitation is one of the most difficult aspects of numerical weather prediction. It is often organized at mesoscales [i.e., a few tens to a few hundreds kilometers; see Fritsch et al. (1986)], which are not well represented by most atmospheric models. Because initial conditions at these scales are not well specified and because the physical processes leading to precipitation are complex and not fully understood (e.g., cloud microphysics, entrainment/detrainment, convective triggering), our ability to predict precipitation has not improved as fast, in the last decades, as our ability to predict mass and temperature fields (Bonner 1989; Olson et al. 1995; Fritsch et al. 1998).

Corresponding author address: Dr. Stéphane Bélair, Recherche en Prévision Numérique, 2121 Trans-Canada Highway, Room 500, Dorval, PQ H9P 1J3, Canada.
E-mail: stephane.belair@ec.ge.ca

The nature of quantitative precipitation forecasts (QPFs) is particularly complex for mesoscale models, with resolution on the order of a few tens of kilometers. At this resolution, now common in regional weather forecasting (Black 1994; Mass and Kuo 1998; Bélair et al. 2000), two types of cloud schemes need to be used concurrently: first, an implicit scheme for the parameterization of subgrid-scale convective activity, and second, an explicit scheme for larger-scale clouds resolved on the model grid scale.

Essentially, the task of the implicit scheme is to trigger deep convective activity at the right time and location, and to vertically stabilize model columns through temperature and humidity tendencies that represent the effect of subgrid-scale condensation and convective eddies. The explicit scheme, on the other hand, takes care of microphysical cloud processes, like condensation, evaporation, and sublimation, that occurs at larger scales resolved by the model.

A realistic balance between these two types of

schemes, implicit and explicit, has been shown to be a key element for the successful simulation of mesoscale convective systems (MCSs; see Zhang et al. 1994; Molinari and Dudek 1992; Hong and Pan 1998). If the implicit scheme is too active and removes too much energy in the convective portion of the weather system, grid-scale condensation in the stratiform region will be underestimated and the model is not likely to capture the internal mesoscale circulations of such systems (Bélair et al. 1995). Conversely, grid-scale condensation could be overestimated and lead to exaggeratedly intense mesoscale circulations if the implicit scheme does not provide enough stabilization in the convective portion of the system (Zhang et al. 1988).

This delicate equilibrium between implicit and explicit schemes changes with resolution. When horizontal resolution increases, a larger portion of the cloud activity spectrum is resolvable on the model grid scale. As a result, the model produces stronger vertical motions, sharper saturated regions, and more intense explicit condensation. It is unclear yet at what resolution the explicitly resolved part of cloud activity starts to dominate to the point that the implicit scheme becomes useless, or worse, detrimental to the simulation of mesoscale weather systems.

An attempt to shed some light on the above uncertainty has been done by Weisman et al. (1997). Their work, which follows a prolonged effort to study squall-line systems using high-resolution numerical modeling (see Weisman et al. 1988; Lafore and Moncrieff 1989; Skamarock et al. 1994), suggests that a minimum grid length of 4 km is necessary for a completely explicit model (i.e., without any convective parameterization) to represent reasonably well the internal structures and mesoscale circulations of a squall line. For lower-resolution models, Weisman et al. (1997) found that the simulated squall lines evolve too slowly and that the scale and intensity of the overturning associated with the convective portion is overestimated. One reason put forward for this slow evolution is related to the cold pool below the leading convective line (see Johnson and Hamilton 1988). At lower resolution, the cold pool is slow to develop, with consequences on the subsequent evolution of the squall line (see Rotunno et al. 1988).

Apart from Weisman et al. (1997), few studies focused on the impact that increasing the horizontal resolution could have on the interactions between implicit and explicit condensation schemes for the simulation of MCSs. Recently, Wang and Seaman (1997) and Gallus (1999) examined the role of resolution on the performance of several convective schemes. But their emphasis was mainly on the objective evaluation of the implicit schemes, and not on the roles of and interactions between the two types of schemes.

The main objective of this study is thus to investigate the impact of increasing or decreasing the horizontal resolution on the roles of and interactions between implicit and explicit condensation schemes. For this purpose, a typical squall line that propagated in the south-central United States during 7–8 May 1995 (see section 2) was simulated with the nonhydrostatic Mesoscale Compressible Community (MC2) model (see section 3) with horizontal resolutions of 50, 18, 6, and 2 km. The sensitivity of the squall line's mesoscale structures to the horizontal resolution is discussed (see section 4), as well as the roles and interactions between the implicit and explicit condensation schemes (see section 5).

2. The 7–8 May 1995 squall line

The MCS chosen for this study occurred over the southern Great Plains on 7–8 May 1995, during the Verification of the Origins of Rotation in Tornadoes Experiment 1995 field campaign (see Rasmussen et al. 1994). During that day, two intense squall lines swept across Kansas and Oklahoma, causing substantial material damage (NCDC 1995).

As shown in Fig. 1, the large-scale environment was favorable for the development and intensification of the two squall lines. A prominent midlevel baroclinic wave and a surface depression near the border between Colorado and New Mexico provided conditions propitious to severe weather. In particular, one should note the destabilizing effect of the low-level advection of warm air from the Gulf of Mexico combined with the midlevel advection of cold air over the southern Great Plains.

The first convective cells of the two MCSs were triggerred around 1600 UTC 7 May near the edge of a dryline located in the Texas panhandle. This initial convection then became more organized and developed into the first squall line, which propagated rapidly toward the northeast (Wang et al. 1996; Magsig and Snow 1998). Of moderate intensity, this first squall line caused less material damages than the one that followed, which was also initialized along the dryline, shortly before 1830 UTC 7 May. In the early stages of this second MCS, several supercells were responsible for severe weather in southwest Oklahoma. Tornadoes were observed in association with some of these supercells as they propagated along the cold outflow produced by the convective activity from the first squall line (Magsig and Snow 1998).

As evidenced by the radar reflectivities shown in Fig. 2, convection in the second system later organized to form a squall line with mesoscale structures typical of the mature phase of such systems (see Johnson and Hamilton 1988; Houze et al. 1989). A narrow line of deep convection was observed at the leading edge of the mesoscale system, with reflectivities of 45–50 dB*Z*, corresponding to precipitation rates of about a few tens of millimeters per hour [according to an empirical *Z*–*R* relationship given in Rogers and Yau (1989)]. It was followed by a broad region of less intense precipitation associated with the trailing anvil (35–45 dB*Z*, i.e., a few mm h^{-1}). The orders of magnitude of precipitation in the convective and trailing anvil regions agree well with

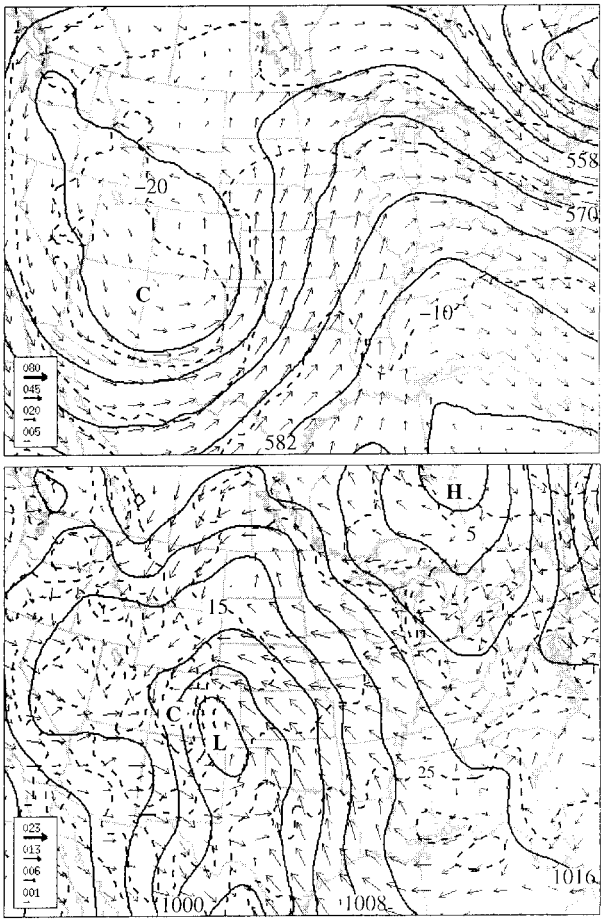

FIG. 1. Large-scale analyses valid at 0000 UTC 8 May 1995. (top) Heights (solid lines, every 6 dm), air temperature (dashed lines, every 5 K), and horizontal winds (kt) at 500 hPa. (bottom) Sea level pressure (solid lines, every 4 hPa), surface air temperature (dashed lines, every 5 K), and surface winds (kt). The letter C indicates a cold region, whereas the letters H and L point to high and low pressure centers.

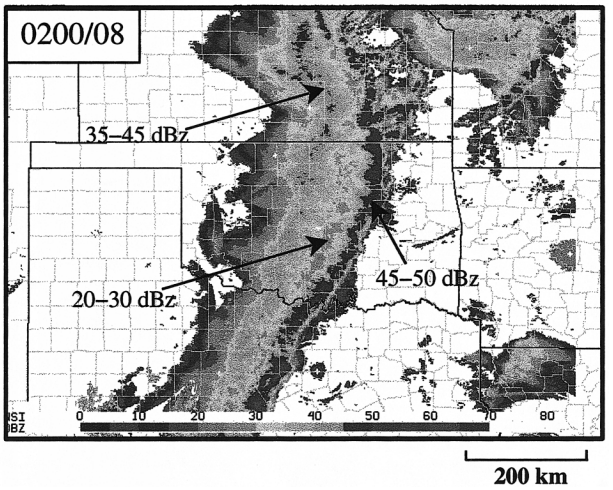

FIG. 2. Plan position indicator (PPI) composite of radar reflectivities (shadings, in dBZ) valid at 0200 UTC 8 May 1995. Reflectivity values for the leading convective line, transition region, and stratiform portion of the squall line are indicated.

surface measurements discussed later in section 5b. In the transition region between the two regimes, the reflectivities were much weaker (i.e., 20–30 dBZ).

3. Modeling strategy

The main focus of this study is to examine the ability of an atmospheric model to realistically simulate the mesoscale structures observed during the mature phase of this second squall line that occurred on 7–8 May. The nonhydrostatic MC2 model (Benoit et al. 1997) is used for this purpose. MC2 is a limited-area model in which the fully compressible Euler equations are integrated using the semi-implicit and semi-Lagrangian numerical techniques. A gird-nesting strategy for the lateral boundary conditions allows high-resolution model integrations over small regions. More details on the main features of this model are given in Table 1.

The main physical processes occurring in the atmosphere are represented in MC2 (see Mailhot et al. 1998 and Table 1). Warming from solar radiation is included following Fouquart and Bonnel (1980), whereas temperature tendencies from infrared radiation are based on Garand (1983). The two radiation schemes (solar and infrared) are fully interactive with simulated clouds. The surface temperature evolves according to the force–restore equation presented in Deardorff (1978), and the

TABLE 1. Summary of MC2.

Dynamics/numerics
Fully compressible Euler equations
Polar stereographic projection on a sphere
Vertical, terrain-following (modified Gal-Chen) coordinate
Helmholtz equation on perturbations of log(pressure ($t + \Delta t$))
Nesting of lateral/upper boundaries for all prognostic variables (sponge zones)
Variable resolution in the vertical
Three time levels ($t - \Delta t$, t, $t + \Delta t$) + filter + off centering
Semi-implicit time scheme
3D semi-Lagrangian scheme
Horizontal and vertical staggering with second-order finite differencing
Implicit $2\Delta x$ filtering of topography due to horizontal staggering
Time-implicit horizontal diffusion on horizontal and vertical velocity, temperature, pressure, and humidity
Physics
Planetary boundary layer based on TKE
Fully implicit vertical diffusion
Stratified surface layer, distinct roughness lengths for momentum and heat/humidity
Force–restore method for land surface processes
Solar/infrared radiation schemes with cloud–radiation interactions based on predicted cloud radiative properties
Shallow convective parameterization
Variety of deep convective schemes (including Kain–Fritsch)
Variety of explicit cloud schemes (including the explicit moisture and Kong–Yau schemes)

exchanges of heat, moisture, and momentum between the surface and the atmosphere depend on the surface layer formulation described in Delage and Girard (1992) and Delage (1997). The vertical diffusion and mixing in the planetary boundary layer is based on vertical diffusivity coefficients that rely on diagnostic mixing lengths and on prognostic turbulent kinetic energy (TKE; Benoit et al. 1989). This one-dimensional turbulence scheme based on TKE is used for all the simulations presented in this study, including the 2-km run in which a three-dimensional treatment of turbulence would be more appropriate.

Several precipitation schemes are available in MC2's physics package. In this study, the deep convection scheme described in Kain and Fritsch (1990, 1993) is used for the implicit condensation. In this scheme, the intensity of parameterized deep convection is proportional to the convective available potential energy (CAPE). Based on Fritsch and Chappell (1980), deep convection is triggered only if low-level upward motion is sufficient to overcome the convective inhibition, that is, the negative energy below the level of free convection on a skew T–log$p$ diagram. The Kain–Fritsch scheme is currently considered for operational implementation in several national centers, including those in Canada, the United States, and France.

For explicit condensation, two schemes are used in this study. The simplest of these schemes is described in Zhang (1989) and is based on the works of Lin et al. (1983), Rutledge and Hobbs (1983), and Hsie et al. (1984). In this scheme, cloud water and ice content, as well as rain and snow, evolve according to prognostic equations that consider a wide variety of microphysical processes, such as autoconversion of cloud water and ice, evaporation, sublimation, depositional growth of ice, etc. The Zhang (1989) explicit scheme has been used with success in mesoscale models with resolutions on the order of 20–25 km to simulate the internal structures of MCSs (Zhang et al. 1989; Bélair et al. 1994). But due to certain simplifying assumptions, the use of this scheme is questionable in models with resolution of a few kilometers or less. One of these assumptions, for instance, is that the liquid and solid phases do not coexist in clouds. The liquid phase is allowed only when air temperature $T_{\text{air}} \geq 0$, and vice versa for the solid phase.

For high-resolution simulations of MCSs, in which simulated circulations are more realistic and more intense, sophisticated cloud microphysics like that included in the Kong and Yau (1997) scheme is required. In this scheme, a wider variety of microphysics mechanisms is included and more cloud variables are determined prognostically (i.e., cloud water, cloud ice, rain, snow, and graupels). It must be mentioned that even though this scheme is likely to be more appropriate for 1–2-km simulations, it is not necessarily so for lower-resolution mesoscale models with resolution of a few tens of kilometers, in which a different level of parameterization might be required.

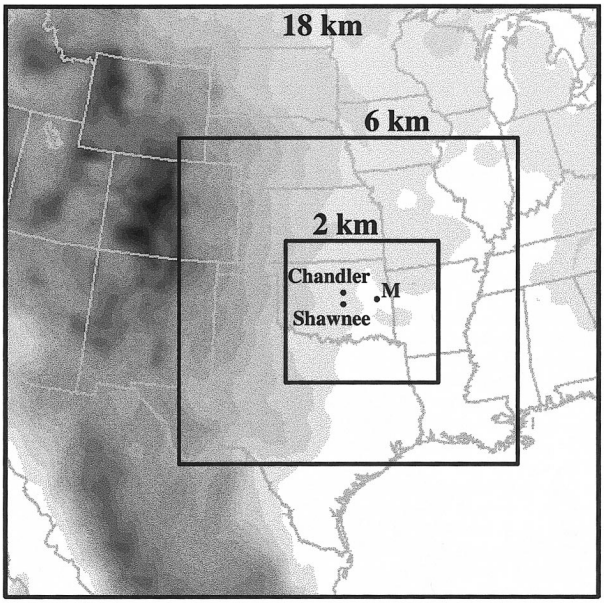

FIG. 3. Integration domains for the 18-, 6-, and 2-km MC2 numerical simulations. The shadings represent topography, with contours every 200 m. The locations of Chandler and Shawnee are also shown. The letter M indicates the position of the points used for the simulated time series of precipitation shown in Figs. 9 and 10.

To examine the impact of horizontal resolution on the simulation of the 7–8 May 1995 squall line, a series of four integrations is performed. The model is first integrated with a resolution of 50 km from 0000 UTC 7 May to 0600 UTC 8 May (30 h). The initial and lateral boundary conditions for this 50-km simulation are provided by the then-operational Canadian Meteorological Center's regional analyses (Chouinard et al. 1994). The three other simulations are performed in a one-way grid-nested mode, with the initial and lateral boundary conditions given by the lower-resolution simulations: (a) the 18-km simulation starts at 1200 UTC 7 May and ends at 0600 UTC 8 May (18 h), (b) the 6-km simulation goes from 1800 UTC 7 May to 0600 UTC 8 May (12 h), and (c) the 2-km simulation is from 2200 UTC 7 May to 0600 UTC 8 May (8 h). To be consistent, the number of vertical levels is increased for higher-resolution experiments: 29 levels are used for the 50- and 18-km simulations, 35 levels for the 6-km run, and 44 levels for the 2-km simulation. In all these configurations, the vertical resolution is greater at low levels and slowly decreases with height with a top level at 30 km above the ground. Time steps of 600, 200, 40, and 15 s are used for the 50-, 18-, 6-, and 2-km runs, respectively. The integration domains for the 18-, 6-, and 2-km simulations are shown in Fig. 3. The domain for the 50-km run includes all of North America (not shown).

The combinations of implicit–explicit schemes that are used at the four horizontal resolutions are given in

TABLE 2. Experimental setup.

Expt	Horizontal resolution (km)	Convective parameterization	Grid-scale condensation scheme
KFEX50	50	Kain–Fritsch	Zhang (1989)
KFEX18	18	Kain–Fritsch	Zhang (1989)
KFKY6	6	Kain–Fritsch	Kong and Yau
KY6	6	None	Kong and Yau
KY2	2	None	Kong and Yau

Table 2. For the 50- and 18-km simulations, the implicit Kain–Fritsch scheme and the Zhang (1989) explicit scheme are used (expts KFEX50 and KFEX18). The Zhang (1989) scheme is used at these ''mesoscale'' resolutions instead of the Kong–Yau scheme because it leads to more realistic simulations of the mesoscale internal structures of the squall line (the comparison is not shown here).

For the 2-km simulation, an implicit scheme is not necessary since the horizontal resolution is sufficient (although marginally) to resolve organized deep convective activity (the scale of the convective band is about 10 km). The 2-km simulation is thus totally explicit, in the sense that no implicit scheme is used. Because of its sophistication, which is appropriate at this scale, the Kong–Yau scheme is used at this resolution (expt KY2).

Of all the resolutions examined in this study, 6 km is certainly the most problematic with respect to the partition of condensation into implicit and explicit processes. On the one hand, this horizontal resolution is not sufficient to properly resolve organized deep activity, so some kind of implicit representation of convective clouds is needed. On the other hand, the resolution is too close to the convective scale, so that no implicit scheme is really suitable, to our knowledge, to represent correctly the effect of subgrid-scale convection, because the separation between the model grid scale and the parameterized subgrid scale is not large enough. For that reason, two experiments were done at this resolution: one with both implicit and explicit schemes (Kain–Fritsch and Kong–Yau, expt KFKY6), and one completely explicit (with the Kong–Yau scheme, expt KY6). As shown in the next section, the simulation of this particular squall line is degraded if no implicit scheme is used.

4. Squall-line mesoscale structures

In general, the model reproduces fairly well the initiation and evolution of the two squall lines that occurred on 7–8 May 1995 even though, as is often observed for real-case simulations, the timing and phase of the convective system are not represented with perfect accuracy. In this case, the two squall lines are initiated too late (about 1–2 h) and too much to the east (about 100 km) as compared to radar observations. These spatial and temporal shifts are found at every stage of the squall lines' evolution.

When initializing MC2 at 1200 UTC 7 May (instead of 0000 UTC 7 May), the phase errors between the observed and simulated squall lines are slightly reduced. But because 1200 UTC is closer to the time of the simulated squall lines, the model has less time to ''adapt'' from the large-scale initial conditions to the mesoscale circulations resolved by the higher-resolution configurations (through nesting from 50- to 18-km grid lengths, then to 6 km, and finally to 2 km). As a result, the mesoscale structures of the two squall lines are poorly represented as compared with those from the simulations using initial conditions at 0000 UTC 7 May. In particular, the first squall line is almost completely missed by the model because it occurs too early in the integration (only 4–5 h after the initial time), and the mesoscale structures of the second squall line are less realistic. Considering that the purpose of this study is mainly to investigate the ability of the mesoscale model to reproduce the mesoscale structures of the second squall line, the phase errors are of secondary importance and we chose to examine the simulations initialized at 0000 UTC 7 May.

The total precipitation rates, including contributions from both implicit and explicit schemes, are shown in Fig. 4 for experiments KFEX50, KFEX18, KFKY6, and KY2. (Results from the completely explicit 6-km simulation—KY6—are discussed later.) For a better evaluation of the model-simulated mesoscale structures during the mature phase of the MCS, outputs valid at 0300 UTC 8 May, that is, 1 h later than the radar reflectivities shown in Fig. 2, are examined (the 1-h lag is for the effect of the simulations' timing errors). Figure 4 shows that MC2 is able to reproduce reasonably well the squall line, at all the resolutions. This is encouraging considering that the simulations were initialized with standard synoptic observations taken more than 20 h before the event, without any special assimilation of mesoscale data.

As expected, smaller-scale details are captured in the higher-resolution simulations. For instance, the 2- and 6-km configurations generate, in agreement with radar observations, distinct convective and trailing anvil regions, while the 18- and 50-km runs only produce a single precipitation band. (Note however that the southern portion of the squall line is not as well represented in the 2-km run because of the proximity of the southern lateral boundary of the integration domain; see Fig. 3.) The positive impact of increased horizontal resolution is also found at the early and dissipating stages of the squall line (not shown). For simplicity's sake, the discussion in this paper concentrates on the mature phase of the weather system.

a. Explicit 2-km simulation (expt KY2)

The precipitation rates for the 2-km simulation (Fig. 4) show that the fully explicit model produces a narrow

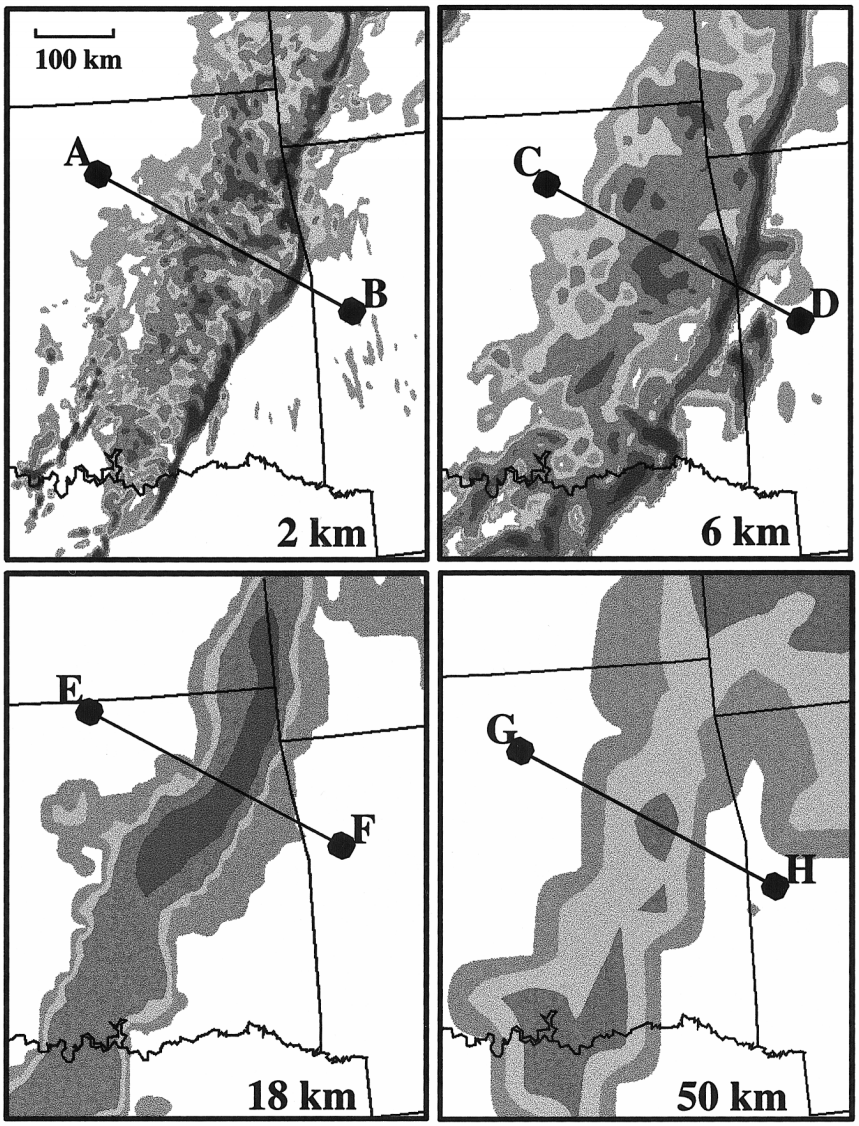

FIG. 4. Total precipitation rates valid at 0300 UTC 8 May 1995 for expts KY2, KFKY6, KFEX18, and KFEX50. The shadings represent precipitation intensities greater than 1, 5, 10, and 25 mm h^{-1}. The letters, from A to H, show the positions of vertical cross sections given in subsequent figures.

and intense convective line at the leading edge of the system with rates greater than 25 mm h^{-1}, followed by a broader region with weaker precipitation (rates of 5–10 mm h^{-1}) associated with the trailing anvil. The transition region, with even weaker precipitation rates, is also captured by the 2-km model. Even though the simulated squall line is too much to the east as compared with the radar images, its phase speed is well captured by the model (i.e., 16 m s^{-1} for the simulation compared with 15 m s^{-1} in reality).

It can also be noted that the simulated leading convective line is narrower and more intense than that observed (cf. Figs. 2 and 4). This problem of the explicit simulation could be related to a misrepresentation of the effect on the smallest resolvable scales (~10 km) of subgrid-scale circulations associated with unresolved convective cells or boundary layer turbulence. Because the horizontal resolution is barely sufficient to resolve the linearly organized leading convective line, the 2-km model does not include the effect of smaller-scale convective cells. This effect may be important, and it is possible that some type of implicit representation of convection is necessary even for models with grid lengths of 2 km. On the other hand, the treatment of subgrid-scale turbulence, not unlike that of deep convection, becomes less well posed as the horizontal resolution increases and the model starts to resolve the larger turbulent eddies in the boundary layer. It is quite possible that a three-dimensional turbulence scheme based on isotropic dissipation would be more appro-

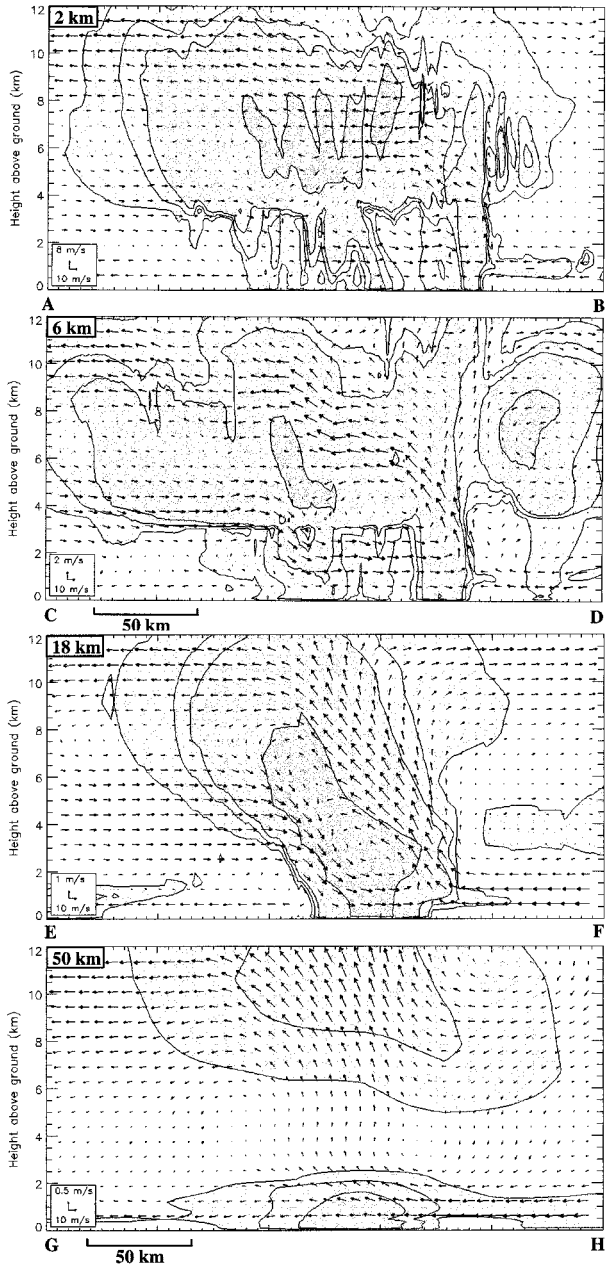

FIG. 5. Vertical cross sections of total cloud water and ice content, superimposed with air motion relative to the squall-line movement, for expts KY2, KFKY6, KFEX18, and KFEX50, valid at 0300 UTC 8 May 1995. The shadings represent regions where total cloud water–ice mixing ratios exceed 0.1, 0.5, 1, and 5 g kg^{-1}. The legends for the wind speed are given in the lower-left corner of the cross sections. The letters, from A to H, indicate the positions of the cross sections end points (see Fig. 4).

priate for this type of resolution (e.g., Smagorinsky 1963).

The vertical cross section in Fig. 5 for the 2-km simulation shows cloud structures and two-dimensional circulations that are consistent with the precipitation field. The updrafts in the leading convective portion of the squall line are intense (with vertical velocities greater than 10 m s^{-1}), narrow (5-10 km), and are responsible for a convective band that extends vertically up to 8–10 km above ground and that contains up to 5 g kg^{-1} of cloud water. The trailing anvil, in contrast, extends rearward for several hundreds of kilometers with cloud water amounts of a few grams per kilogram. In this region, a slightly ascending front-to-rear (FTR) current carries warm and humid air that originates from the boundary layer ahead of the squall line and that is deposited in the trailing anvil by the intense leading convective updrafts (Houze et al. 1989; Zhang and Cho 1992). Just below, another current from the rear-to-front (RTF) transports cooler and drier air into the MCS. This RTF flow slowly descends toward the surface, except at a few locations where the downward motion is stronger due to localized evaporation of precipitation below the anvil clouds (Smull and Houze 1987; Zhang et al. 1989).

Unfortunately, these mesoscale circulations could not be directly compared against actual measurements for this particular squall line. But the structures described above are consistent with conceptual models and idealized simulations of this type of system (see Weisman et al. 1988; Houze et al. 1989), other high-resolution simulations (e.g., Hemler et al. 1991), and remarkably resemble those from the radar observations presented in Heymsfield et al. (1999). It thus seems clear that the explicit 2-km simulation produce physically realistic mesoscale structures for this squall line and that we are justified to use this simulation as ''synthetic data'' to evaluate the performance of the lower-resolution configurations.

b. The 6-km simulations (expts KFKY6 and KY6)

The 6-km simulation with the Kain–Fritsch convective scheme and the Kong–Yau condensation scheme (expt KFKY6) has fewer smaller-scale details than the 2-km run, but the results remain satisfactory (cf. Figs. 2 and 4). At this resolution, the model is still able to produce distinct regions for the convective and trailing anvil portions of the MCS, with the transition zone in between. The two regions are slightly larger than in the 2-km simulation, which seem to correspond better with radar observations. The phase speed of the squall line is also well reproduced by the 6-km model (i.e., 16 m s^{-1} during the mature phase).

A vertical cross section reveals that the main two-dimensional mesoscale structures and circulations are also reproduced by the 6-km model (see Fig. 5). In particular, one can recognize in this cross section the leading convective line followed by the mesoscale anvil. One should note, however, that the convective band is less intense, wider, and not as deep as that produced in the 2-km simulation. Except for this and the decreased variability of precipitation associated with the trailing

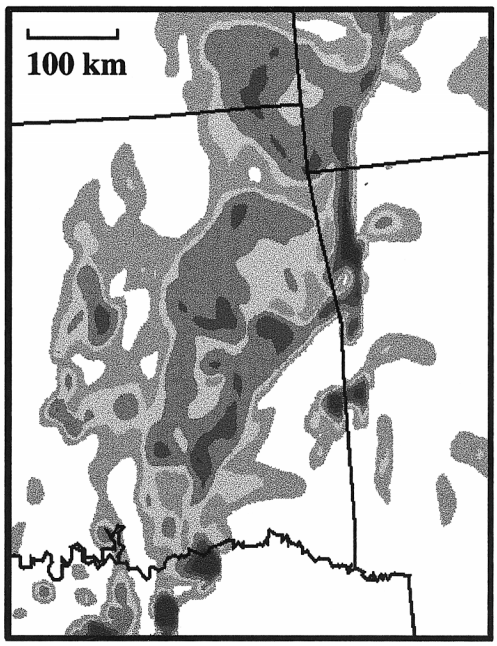

FIG. 6. Same as Fig. 4 but for expt KY6 (see Table 2), in which no convective parameterization scheme is used.

anvil, the mesoscale structures appear to be as realistic as those produced by the 2-km explicit model.

One may wonder if a fully explicit version would have as much success at 6-km resolution. Figure 6 clearly shows that this is not the case. A 6-km explicit version of MC2 (expt KY6) represents well the stratiform portion of the MCS, but is not able to sustain long enough the leading convective line that, by 0300 UTC 8 May, is already dissipated. It thus seems, as anticipated, that a horizontal resolution of 6 km is not sufficient to explicitly represent deep convection on the grid scale. At 6 km, grid-scale circulations are not ''fast'' enough to reproduce accurately the vertical stabilization resulting from convective overturning, with both upward and downward branches, observed at the leading convective edge of the MCS.

c. The 18-km simulation (expt KFEX18)

The total precipitation rates for the mature phase of the squall line from the 18-km simulation (expt KFEX18) are quite different from those produced by the higher-resolution configurations (see Fig. 4). At a resolution of 18 km, the model is no longer able to represent the two distinct regions for the convective and anvil portions of the MCS. Instead, only one single precipitation band is generated, which is not as wide as the trailing anvils in the 2- and 6-km runs, but more intense, with precipitation rates greater than 25 mm h^{-1}.

It could be argued that part of these differences with the higher-resolution simulations can be attributed to the use of the Zhang (1989) scheme, instead of the Kong–Yau scheme. But sensitivity experiments, not shown here, indicate that the general behavior of these two condensation schemes is not very different. With either scheme, the model produces a single, intense band of precipitation. The differences between the simulations using the Zhang (1989) and Kong–Yau schemes are more related to the mesoscale organization of the squall line. When using the Zhang (1989) condensation scheme, the model is able to produce relatively realistic mesoscale circulations, such as the FTR–RTF couplet in the trailing anvil. With the Kong–Yau scheme, however, these structures are not as well represented and the squall line dissipates too rapidly (not shown). The different behavior of the two schemes is certainly related to specific assumptions and strategies used in their construction. In the present case, the Zhang (1989) scheme seems to be better adapted for models with 20–50-km horizontal resolution than the Kong–Yau scheme, which was conceived for high-resolution explicit modeling, with more realistic vertical motions and saturation behaviors.

A vertical cross section during the mature phase of the 18-km run's squall line also shows, not surprisingly, many differences with the higher-resolution simulations (see Fig. 5). First, the 18-km model does not represent, on the grid scale, the leading convective band. The grid-scale vertical motion is not sufficient in this case to generate explicit condensation. All the condensation processes in that portion of the MCS are parameterized.

In the trailing anvil, by contrast, the circulations associated with the FTR–RTF couplet are quite intense and dominate up to 12 km above ground. Grid-scale condensation in this region leads to large precipitation rates, as seen in Fig. 4. Even if this type of circulation does not compare well with those produced in the 2-km explicit simulation, this squall-line simulation using a mesoscale model remains acceptable if one considers the relatively low resolution of the model. In fact, this simulation compares well against results reported in the last decade using similar mesoscale resolutions (20–25 km) (see Zhang et al. 1994; Bélair et al. 1994; Bélair and Zhang 1997). The FTR and RTF flows are represented by the model, as well as other features such as a wake low at the rear of the trailing anvil and a mesohigh below the convective line (not shown).

d. The 50-km simulation (expt KFEX50)

The precipitation field shown in Fig. 4 for the 50-km simulation (expt KFEX50) exhibits several features similar to the 18-km results, such as the single band of precipitation. The intensity, however, is much less with the 50-km configuration.

The internal structures of the simulated MCS are also quite different from the higher-resolution simulations (Fig. 5). With a resolution of 50 km, the model does not produce the FTR–RTF couplet in the trailing anvil. Furthermore, the clouds represented explicitly on the

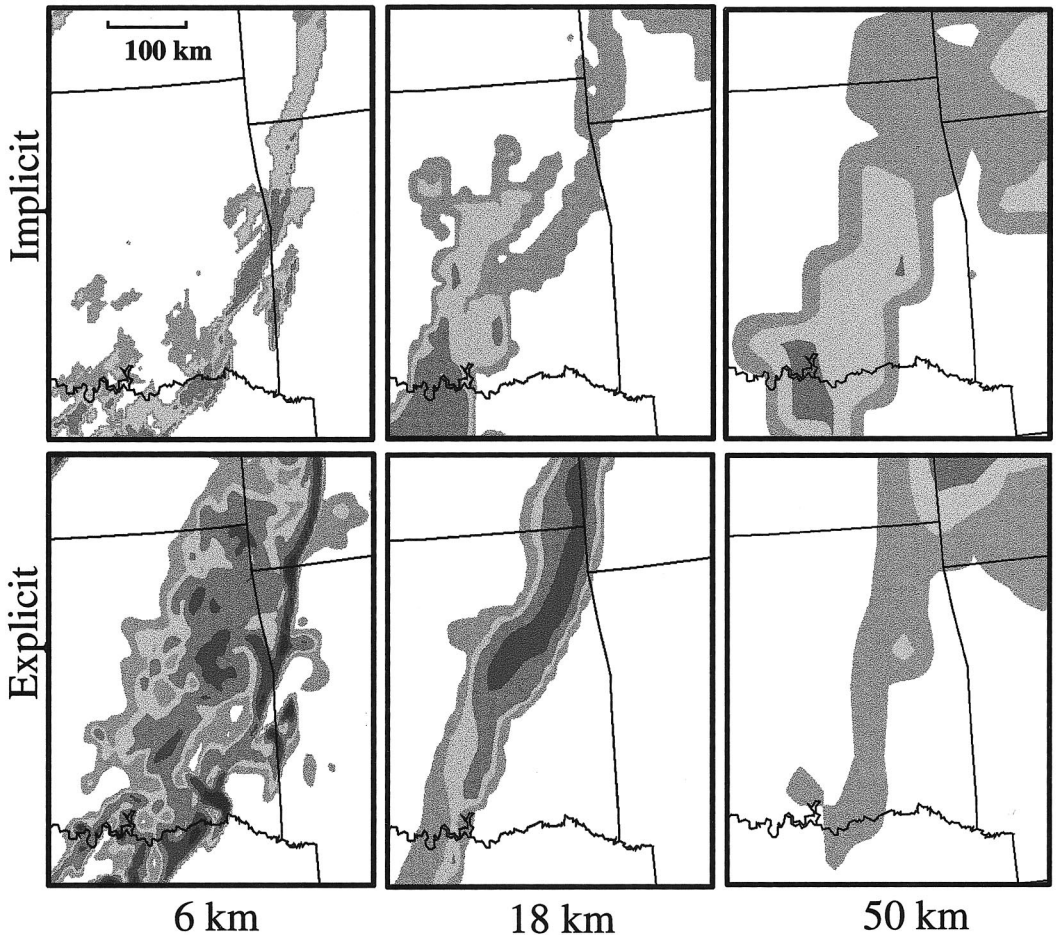

FIG. 7. Implicit and explicit precipitation rates valid at 0300 UTC 8 May 1995 for expts KFKY6, KFEX18, and KFEX50. The shadings represent precipitation intensities greater than 1, 5, 10, and 25 mm h^{-1}.

grid scale are even less realistic than those of the 18-km simulation. They occur at two separate locations: (i) at low levels because of the lifting of boundary layer warm and moist air due to the enhanced convergence related to cooling in the parameterized downdrafts, and (ii) in the mid-to upper troposphere in relation with upward motion and cloud water detrainment associated with parameterized convection. Therefore, in the same manner that 18 km is too coarse a resolution to resolve the leading convective line, 50-km resolution is not sufficient to resolve the mesoscale circulations in the trailing anvil, which thus have to be parameterized, one way or another.

5. Implicit and explicit precipitation

a. Partition between implicit and explicit condensation

The precipitation fields shown in Fig. 4 for experiments KFKY6, KFEX18, and KFEX50 are the joint result of both implicit and explicit condensation. Due to the nature of their physical parameterizations, the implicit and explicit schemes should logically represent the cloud activity in the convective and anvil regions of the MCS, respectively. Figure 7 shows that the partitioning of precipitation into implicit and explicit components varies with resolution. With increasing resolution, the relative contribution of the explicit scheme increases, and vice versa for the implicit scheme.

For instance, most of the precipitation for the 50-km simulation is produced by the Kain–Fritsch implicit scheme. At this resolution, the Zhang (1989) explicit scheme only generates a narrow precipitation band, less intense than the implicit one. It is interesting to note that even though the explicit band occurs toward the rear of the MCS, it is not separated from the implicit precipitation. That is, both the implicit and explicit schemes are acting over the same region. Moreover, the implicit band of precipitation (associated with convective activity) is wider than the explicit band (anvil region), which does not correspond to the observed structure of the MCS. This different partitioning occurs be-

cause the model is not able, as already mentioned, to capture explicitly the mesoscale circulations of the squall line such as the FTR–RTF couplet. The effect of the mesoscale circulations in the trailing anvil must then be represented implicitly. Unfortunately, the Kain–Fritsch scheme was not constructed with this aspect in mind, and its ability to represent the effect of mesoscale circulations such as the FTR–RTF couplet may not be optimal.

For the 18-km simulation, the roles of the implicit and explicit schemes concerning precipitation's partitioning is more realistic. As expected, the precipitation band from the Kain–Fritsch implicit scheme is narrower and occurs at the leading edge of the MCS. The Zhang (1989) explicit scheme, on the other hand, is responsible for the broader precipitation band at the rear of the squall system. It could be argued, however, that the respective intensities of the two types of precipitation are the reverse of what would be expected. If we consider that the implicit and explicit schemes represent, respectively, unresolved deep convective activity and grid-scale condensation (which occurs on the mesoscale), it follows that implicit (i.e., convective) precipitation should be more intense than explicit (i.e., mesoscale) precipitation. The opposite occurs for the 18-km simulation. At this resolution, the grid-scale circulations become unrealistically intense because hydrostatic scales are trying to respond to convective instability.

In the 6-km simulation (expt KFKY6), the implicit precipitation at the leading convective line is more intense and narrower than at 18 km, in better agreement with radar observations. Precipitation in the trailing anvil of the MCS is also better represented by the explicit Kong–Yau scheme. This precipitation region is wider and less intense than in the 18-km simulation.

One disturbing aspect of the KFKY6 simulation, though, concerns the simultaneous activation of both implicit and explicit schemes for the leading convective precipitation. Even more troubling is that the explicit contribution in this region is greater than that from the implicit scheme. Because 6 km is sufficient to partly resolve the intense circulations at the leading convective line (see Fig. 5), this part of the MCS is both ''parameterized'' and ''resolved'' at the same time. In this context, the closure assumptions at the core of the Kain–Fritsch convective scheme (and, in fact, of all convective schemes) do not hold. The problem becomes ill-posed at this resolution. This does not negate the fact, nevertheless, that the simulation of the mesoscale structures of the 7–8 May squall line are more realistic at 6 km than at 18 km, at which resolution the basis of implicit–explicit partitioning of precipitation seems to have a better physical foundation.

b. Time series of precipitation

Another means of looking at the respective roles of implicit and explicit condensation schemes consists of comparing simulated time series of precipitation with measurements at surface stations. Because atmospheric model QPFs are now frequently used to drive surface and hydrological models, the accurate prediction of the phase, timing, and amount of precipitation becomes crucial.

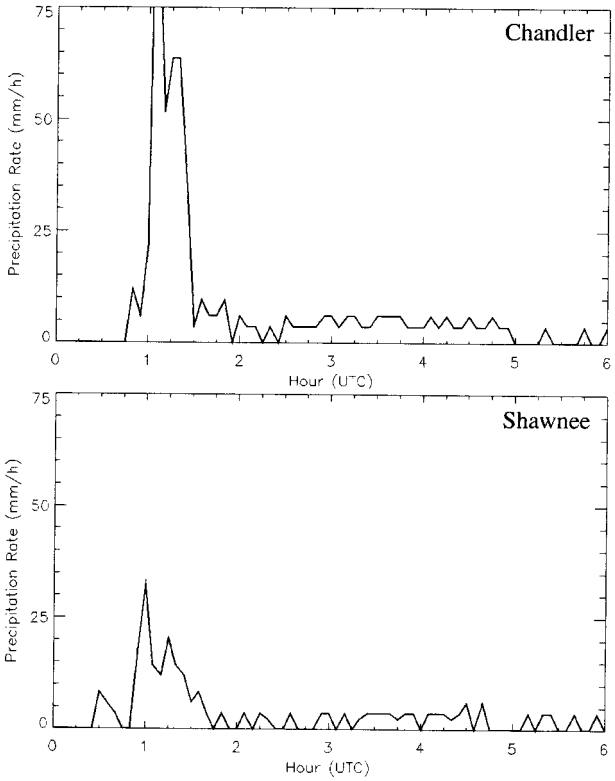

FIG. 8. Observed time series of precipitation rates (mm h^{-1}) at Chandler and Shawnee, two locations in central OK. The hours are in UTC, for 8 May 1995. The locations of Chandler and Shawnee are shown in Fig. 3.

Figure 8 shows time series of precipitation rates observed at Shawnee and Chandler, located in central Oklahoma (see Fig. 3). The rain rates were calculated from 5-min accumulations (mean rate over that period). These two surface stations were chosen to provide a picture of the temporal evolution of precipitation for regions located near the central portion of the squall line. The conclusions formulated from the results below are also valid for the northern and southern portions of the squall system.

For the two stations, a short period (~30–40 min) of intense precipitation was observed, followed by a longer period (a few hours) of weaker precipitation. The intensity of convective precipitation varied between 20 and 35 mm h^{-1} at Shawnee to about 60–80 mm h^{-1} at Chandler; for the trailing anvil region, the precipitation was more uniform with rates of about 5 mm h^{-1} at both locations. The large differences between the early precipitation rates at the two stations confirm the small-scale variability of convective activity, which is not al-

ways captured by the composite radar images. Radar reflectivities (Fig. 2) and observations at other surface stations indicate that the precipitation rates recorded at Chandler are more representative of the average typical severity of precipitation along the convective line.

The precipitation rates in the central portion of the simulated squall lines for experiments KY2, KFKY6, KFEX18, and KFEX50 are shown in Fig. 9. Because of the phase errors for the simulated squall systems, the grid points chosen for the comparison against observations do not coincide with either Shawnee or Chandler. Rather, they are located in eastern Oklahoma, in order to better compare with observations (see Fig. 3). Also, the timescales on the *x* axis of Fig. 9 were translated so that the observed and simulated peaks of convective precipitation could match.

The first panel of Fig. 9 shows that the 2-km explicit model represents reasonably well the temporal evolution of precipitation in the central portion of the squall line. Intense precipitation first occurs for a period of about 30 min, followed by weaker precipitation for approximately 4 h. The simulated rain rates are in good agreement with observations at Shawnee and Chandler for the convective line (between 25 and 75 mm h^{-1}), but are overestimated in the trailing anvil (15 vs 5 mm h^{-1}).

The same sequence of convective and stratiform precipitation is also reproduced by the 6-km model (expt KFKY6; see the second panel of Fig. 9), but with less accuracy. In agreement with Fig. 7, the time series show that most of the precipitation is produced by the explicit scheme, and that both implicit and explicit schemes are active simultaneously in the convective region. The convective period is slightly too long (about 1 h), and several ''pulsations'' modulate the precipitation rates, with periods of about 30 min. Because of these pulsations, which are not observed, the abrupt transition between the convective and stratiform modes is not as obvious as it is in the 2-km run or in the observations. A deeper investigation of these pulses reveals that they are associated with eddies occurring on the smallest resolvable scale of the model. This provides further evidence that 6 km is not sufficient to completely resolve the small-scale circulations occurring in the convective portion of the MCS.

In contrast with observations and higher-resolution results, precipitation in the 18-km simulation is much more intense in the trailing anvil region than in the convective zone (see Fig. 9). In this simulation, precipitation in the convective line is entirely parameterized by the implicit scheme and is very weak compared to observations (smaller than 5 mm h^{-1}). Because the implicitly produced precipitation represents the mean effect of deep convection over a model grid area (18 km $\times$ 18 km in the present case), it has to be much weaker than precipitation locally generated by the subgrid-scale convective elements themselves (i.e., a few tens of mm h^{-1}).

As shown in Figs. 7 and 9, most of the intense anvil

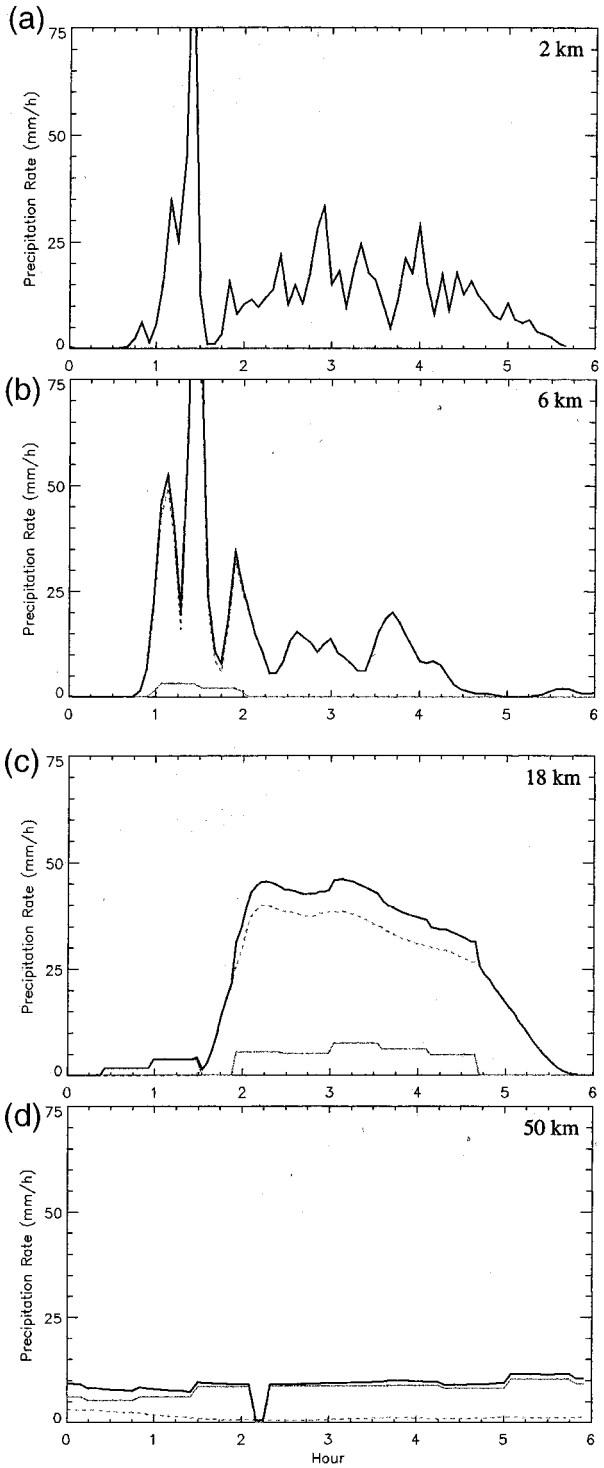

FIG. 9. Time series of precipitation rates (mm h^{-1}) from expts KY2, KFKY6, KFEX18, and KFEX50 for points in eastern Oklahoma over which the central portion of the squall line passed (see Fig. 3). Precipitation from implicit and explicit condensation is indicated by the full and dashed gray lines, respectively. Total precipitation (implicit plus explicit) is shown by the full black lines. The time in hours does not necessarily correspond to the UTC hour for 8 May 1995, since the results were translated in time in order to fit all the maxima of simulated precipitation (associated with the convective portion of the squall line) with observations (see Fig. 8).

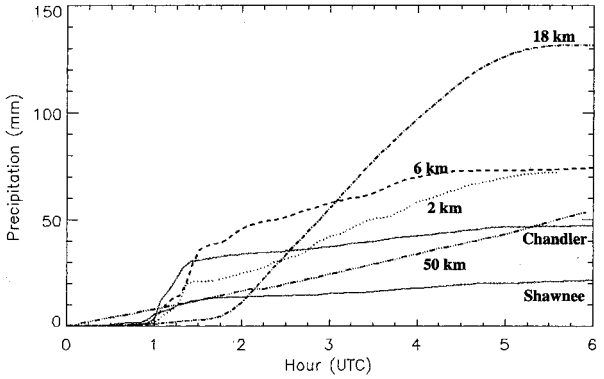

FIG. 10. Observed and simulated accumulations of precipitation (mm). The full gray lines represent the precipitation accumulations observed at Chandler and Shawnee between 0000 and 0600 UTC 8 May 1995. The black dashed lines show the precipitation accumulations for expts KY2, KFKY6, KFEX18, and KFEX50 for the same points and time periods that were used in Fig. 9.

TABLE 3. Rainfall accumulations.

	Total precipitation (mm)	Precipitation in the training anvil (%)
Shawnee	22	45
Chandler	47	36
KY2	74	73
KFKY6	74	53
KFEX18	132	96
KFEX50*	55	—

* No spatial separation between the convective and anvil regions could be found for this simulation. Also, only part of the simulated weather system is included in the 6-h period.

precipitation in the 18-km simulation is produced by the Zhang (1989) explicit scheme. For this configuration, the horizontal resolution is barely sufficient to resolve the internal mesoscale circulations in the trailing anvil of the MCS, such as the FTR–RTF flows. At this resolution, the FTR–RTF couplet is in fact a single large eddy represented at the small end of the model's resolvable scales (see Fig. 5). Because the effect of the energy cascade toward smaller, unresolved scales is not perfectly represented in the model (through the different physical parameterizations), circulations occurring at the smallest resolvable scales could be unrealistic. This translates, in this case, into an exaggerately intense FTR–RTF couplet, which leads to huge amounts of precipitation.

The precipitation time series for the 50-km simulation are lacking in mesoscale structures as compared to those produced by the other configurations (see the bottom panel of Fig. 9). Because the simulated weather system is at larger-scale, the rain rates are almost flat for the chosen 6-h period. As shown in Fig. 7, most of the precipitation is subgrid scale at this resolution.

Observed and simulated accumulations of precipitation for the same 6-h period are given in Fig. 10. Observations at Shawnee and Chandler show a swift increase of accumulated rain during the convective stage (~10 mm in Shawnee and ~30 mm in Chandler, in about 30 min), followed by a longer period of more gradual increase (~10 mm in Shawnee and ~15 mm in Chandler, in about 4 h). The anvil portion of the MCS thus contributes approximately 35%–45% of the total precipitation (see Table 3), in agreement with other observational studies (Houze 1977; Johnson and Hamilton 1988).

The rapid rainfall accumulation in the leading portion of the squall system is well simulated by the 2- and 6-km configurations (expts KY2 and KFKY6). They produce, respectively, about 20 and 35 mm of rainfall accumulation during this period (see Fig. 10). In the trailing anvil, though, the rainfall accumulations are overestimated; that is, the model produces about 50 and 40 mm for the 2- and 6-km runs. As a consequence, the two model configurations produce rainfall accumulations that are about twice as large as those observed (see Table 3). This overestimation is even greater in the 18-km simulation, in which more than 95% of the total rainfall occurs during the stratiform period. The total rainfall for the 18-km simulation is on the order of 130 mm, which is 3–5 times larger than the observations. Finally, it is interesting to note that the accumulation from the 50-km model is more consistent with observations, even though it does not reproduce the internal mesoscale structures of the MCS (see Figs. 4 and 5). It must be kept in mind, though, that the 6-h period is not long enough to contain all the precipitation associated with the simulated weather system (in contrast to the higher-resolution simulations in which the MCS occurs on a smaller scale). Precipitation falling before and after the 6-h period is not accounted for in Fig. 10.

What could possibly explain this systematic overestimation of accumulated rainfall produced by all the model configurations tested in this study? We expect that incorrect initial conditions (especially for low-level humidity and temperature) could be responsible for part of the errors. But they are unlikely to account for an overestimation by a factor of 2–5.

As already discussed, we believe that the rainfall overestimation by the 18-km model is due, for the most part, to an incorrect representation of the FTR–RTF couplet in the trailing anvil of the MCS. By increasing the horizontal resolution to 6 and 2 km, the meso- and smaller-scale structures are better represented, and the precipitation errors are reduced. The remaining problems in the anvil region for the 2- and 6-km simulations are related, in our opinion, to a resolution that is still inadequate to represent properly the convective activity at the leading edge of the system. Because of the interdependence between the two precipitation regions in squall lines, it is conceivable that a more realistic representation of convection could lead to better simulations of precipitation associated with the trailing anvil. This aspect could be evaluated, for example, with even

higher-resolution simulations of the squall line, on the order of a few hundreds of meters. This aspect is currently being examined.

6. Summary and conclusions

The results presented in this study show the impact of increasing or decreasing the horizontal resolution on the simulation of the mesoscale internal structures of a midlatitude squall line that occurred on 7–8 May 1995. For this case, an explicit 2-km version of the atmospheric MC2 model is found to realistically reproduce the meso- and small-scale features of this MCS, such as the intense upward motion in the convective band, the wide trailing anvil cloud region, and the associated FTR ascending and RTF descending flows. This explicit high-resolution simulation is used as a control run to evaluate the performance of lower-resolution configurations.

As the horizontal resolution is decreased, the ability of the model to capture the mesoscale internal structures of the squall line is reduced. At 6 km, both the convective and anvil regions of the MCS are still represented by the model, but the leading convective band is less realistic than for the explicit 2-km run: it is wider, shallower, and less intense. When decreasing further the resolution to 18 km, the convective band is not resolved at all, and its effect on precipitation and vertical stabilization has to be parameterized. At this resolution, the mesoscale circulations in the trailing anvil are still represented on the model grid scale, but are too vigorous (FTR and RTF flows). At 50 km, finally, neither the convective nor the anvil regions are resolved by the model.

The impact of resolution on the partition of condensation into implicit and explicit components is also examined in this study. At 50 km, most of precipitation is subgrid scale, that is, produced by the implicit condensation scheme. As the resolution increases, the MCS circulations are better resolved, and more precipitation occurs at the grid scale. At 18 km, the partition of precipitation is physically correct, in the sense that the small-scale convective activity is taken care of by the implicit scheme, while the broader trailing anvil clouds are represented by the explicit scheme. Yet, the relative intensities of precipitation in these two regions are unrealistic. Most of the simulated rainfall occurs in the anvil region, which is just the reverse of what has been observed. A more reasonable balance between convective and anvil precipitation is restored with the 6-km simulation, even though the implicit–explicit partition of precipitation is ambiguous at this resolution.

This ambiguity arises from the need, even at 6 km, to use an implicit scheme to represent subgrid-scale convective activity, as shown by results from experiment KY6. The explicit circulations, which try to mimic the rapid overturning associated with deep convection, are too large in space and too slow in time to represent correctly this effect on the grid scale. As previously emphasized in the litterature (e.g., Frank 1983; Molinari and Dudek 1992), use of any implicit schemes at this type of resolution (between 3 and 10 km) is in violation of their fundamental assumptions and closure hypotheses. At 6 km, the resolution is so close to the convective scale that the leading convective band is *coincidentally* resolved and parameterized by the model. Because of the lack of scale separation between the convective and grid scales, the results obtained from models with this type of resolution must be examined cautiously, even though they appear to be physically realistic. This necessity of using an implicit scheme even at this relatively high resolution should encourage us in trying to find more appropriate ways to represent the effect of unresolved convective activity in atmospheric models with horizontal resolutions in the gap between cloud resolving models (i.e., ~100 m) and mesoscale models (10 km or more).

An intriguing aspect revealed in this study is the significant overestimation of rainfall accumulation for all the tested configurations. With an overprediction factor of 3–5, the 18-km configuration is the worst for this particular case study. The intense precipitation at this resolution is related to the misrepresentation of the mesoscale circulations in the stratiform region (the FTR and RTF flows). Even if the amounts are reduced as the resolution is increased, the 2- and 6-km configurations also overestimate rainfall accumulations. It is hypothesized that this overprediction of QPF is linked to an imperfect representation of the convective activity at the leading edge of the MCS, even at 2-km resolution. Subkilometer simulations of the squall line would be necessary to examine this aspect. Work in this direction is currently being done.

It must be mentioned that the imperfect initial conditions could also be responsible, partly, for the rainfall overestimation. QPFs also depend on the choice of convective parameterization scheme (Gallus 1999; Bélair et al. 2000). The Kain–Fritsch scheme, used in all the experiments of this study, is based on removal of CAPE and determination of upward and downward convective mass fluxes. This scheme allows a wider scale of interactions, which favors the development of grid-scale mesoscale circulations (see Zhang et al. 1994). Other convective schemes, like Betts–Miller or Kuo-type schemes, remove more energy implicitly and may lead to smaller amounts for total precipitation. The cost of this reduction, however, is less-realistic mesoscale circulations (see Bélair et al. 1994).

The purpose of this study was mainly to discuss the physical mechanisms explaining the influence of horizontal resolution on the simulation of mesoscale internal structures and precipitation in a squall line. The improvements that were found in the mesoscale structures and precipitation patterns of the squall line encourage us to use the modeling approach described in this study for operational forecasting of precipitating weather sys-

tems. A collaborative project between the Meteorological Research Branch (MRB) and the Canadian Meteorological Center (CMC) of the Meteorological Service of Canada is now under way to develop a high-resolution forecasting system, with a nesting strategy similar to that described in this study. Several high-resolution domains with resolution on the order of 2–3 km could be used to cover the main populated areas of Canada. Objective evaluations based on a large number of cases could then be conducted in order to more fully examine the effect of resolution on precipitation biases in atmospheric models.

Acknowledgments. We wish to thank M. Desgagné and P. Pellerin (MRB) for their precious help with the MC2 model. Also, the expertise of B. Bilodeau (MRB) with MC2's physics package is greatly appreciated. Many discussions with A. Méthot (CMC) on various aspects of this study (e.g., triggering of deep convection, implicit–explicit partitioning of precipitation, etc.) were also very helpful. Finally, we wish to acknowledge the contribution of J. S. Kain and one anonymous reviewer, whose comments were quite helpful in significantly improving the quality of the paper.

REFERENCES

Bélair, S., and D.-L. Zhang, 1997: A numerical study of the along-line variability of a frontal squall line during PRE-STORM. *Mon. Wea. Rev.*, **125,** 2544–2561.

——, ——, and J. Mailhot, 1994: Numerical prediction of the 10–11 June 1985 squall line with the Canadian regional finite-element model. *Wea. Forecasting,* **9,** 157–172.

——, ——, and ——, 1995: Numerical prediction of an intense convective system associated with the July 1987 Montreal flood. Part II: A trailing stratiform rainband. *Atmos.–Ocean,* **33,** 475–500.

——, A. Méthot, J. Mailhot, B. Bilodeau, A. Patoine, G. Pellerin, and J. Côté, 2000: Operational implementation of the Fritsch–Chappell scheme in the 24-km Canadian regional model. *Wea. Forecasting,* **15,** 257–274.

Benoit, R., J. Côté, and J. Mailhot, 1989: Inclusion of a TKE boundary layer parameterization in the Canadian regional finite-element model. *Mon. Wea. Rev.,* **117,** 1726–1750.

——, M. Desgagné, P. Pellerin, S. Pellerin, Y. Chartier, and S. Desjardins, 1997: The Canadian MC2: A semi-Lagrangian, semi-implicit wideband atmospheric model suited for finescale process studies and simulation. *Mon. Wea. Rev.,* **125,** 2382–2415.

Black, T. L., 1994: The new NMC mesoscale Eta model: Description and forecast examples. *Wea. Forecasting,* **9,** 265–278.

Bonner, W. D., 1989: NMC overview: Recent progress and future plan. *Wea. Forecasting,* **4,** 275–285.

Chouinard, C., J. Mailhot, H. L. Mitchell, A. Staniforth, and R. Hogue, 1994: The Canadian regional data assimilation system: Operational and research applications. *Mon. Wea. Rev.,* **122,** 1306–1325.

Deardorff, J. W., 1978: Efficient prediction of ground surface temperature and moisture, with inclusion of a layer of vegetation. *J. Geophys. Res.,* **83,** 1889–1903.

Delage, Y., 1997: Parameterising sub-grid scale vertical transport in atmospheric models under statically stable conditions. *Bound.-Layer Meteor.,* **82,** 23–48.

——, and C. Girard, 1992: Stability functions correct at the free convection limit and consistent for both the surface and Ekman layers. *Bound.-Layer Meteor.,* **58,** 19–31.

Fouquart, Y., and B. Bonnel, 1980: Computations of solar heating of the earth's atmosphere: A new parameterization. *Contrib. Atmos. Phys.,* **53,** 35–62.

Frank, W. M., 1983: The cumulus parameterization problem. *Mon. Wea. Rev.,* **111,** 1859–1871.

Fritsch, J. M., and C. F. Chappell, 1980: Numerical prediction of convectively driven mesoscale pressure systems. Part I: Convective parameterization. *J. Atmos. Sci.,* **37,** 1722–1733.

——, R. J. Kane, and C. R. Chelius, 1986: The contribution of mesoscale convective weather systems to the warm-season precipitation in the United States. *J. Climate Appl. Meteor.,* **25,** 1333–1345.

——, and Coauthors, 1998: Quantitative precipitation forecasting: Report of the Eighth Prospectus Development Team, U.S. Weather Research Program. *Bull. Amer. Meteor. Soc.,* **79,** 285–299.

Gallus, W. A., Jr., 1999: Eta simulations of three extreme precipitation events: Sensitivity to resolution and convective parameterization. *Wea. Forecasting,* **14,** 405–426.

Garand, L., 1983: Some improvements and complements to the infrared emissivity algorithm including a parameterization of the absorption in the continuum region. *J. Atmos. Sci.,* **40,** 230–244.

Hemler, R. S., F. B. Lipps, and B. B. Ross, 1991: A simulation of a squall line using a nonhydrostatic cloud model with a 5-km horizontal grid. *Mon. Wea. Rev.,* **119,** 3012–3033.

Heymsfield, G. M., J. B. Halverson, and I. J. Caylor, 1999: A wintertime Gulf coast squall line observed by EDOP airborne Doppler radar. *Mon. Wea. Rev.,* **127,** 2928–2950.

Hong, S.-Y., and H.-L. Pan, 1998: Convective trigger function for a mass-flux cumulus parameterization. *Mon. Wea. Rev.,* **126,** 2599–2620.

Houze, R. A., 1977: Structure and dynamics of a tropical squall line system. *Mon. Wea. Rev.,* **105,** 1540–1567.

——, S. A. Rutledge, M. I. Biggerstaff, and B. F. Smull, 1989: Interpretation of Doppler weather radar displays of midlatitude mesoscale convective systems. *Bull. Amer. Meteor. Soc.,* **70,** 608–619.

Hsie, E.-Y., R. A. Anthes, and D. Keyser, 1984: Numerical simulation of frontogenesis in a moist atmosphere. *J. Atmos. Sci.,* **41,** 2581–2594.

Johnson, R. H., and P. J. Hamilton, 1988: The relationship of surface pressure features to the precipitation and airflow structure of an intense midlatitude squall line. *Mon. Wea. Rev.,* **116,** 1444–1472.

Kain, J. S., and J. M. Fritsch, 1990: A one-dimensional entraining/detraining plume model and its application in convective parameterization. *J. Atmos. Sci.,* **47,** 2784–2802.

——, and ——, 1993: Convective parameterization for mesoscale models: The Kain–Fritsch scheme. *The Representation of Cumulus Convection in Numerical Models, Meteor. Monogr.,* No. 46, Amer. Meteor. Soc., 165–170.

Kong, F., and M. K. Yau, 1997: An explicit approach to microphysics in MC2. *Atmos.–Ocean,* **35,** 257–291.

Lafore, J.-P., and M. W. Moncrieff, 1989: A numerical investigation of the organization and interaction of the convective and stratiform regions of tropical squall lines. *J. Atmos. Sci.,* **46,** 521–544.

Lin, Y.-L., R. D. Farley, and H. D. Orville, 1983: Bulk parameterization of the snow field in a cloud model. *J. Climate Appl. Meteor.,* **22,** 1065–1092.

Magsig, M. A., and J. T. Snow, 1998: Long-distance debris transport by tornadic thunderstorms. Part I: The 7 May 1995 supercell thunderstorm. *Mon. Wea. Rev.,* **126,** 1430–1449.

Mailhot, J., and Coauthors, 1998: Scientific description of RPN physics library. Version 3.6, Recherche en Prévision Numérique, 188 pp. [Available from RPN, 2121 Trans-Canada, Dorval, PQ H9P 1J3, Canada; also online at http://www.cmc.ec.gc.ca/rpn/physic98.pdf.]

Mass, C. F., and Y.-H. Kuo, 1998: Regional real-time numerical weather prediction: Current status and future potential. *Bull. Amer. Meteor. Soc.,* **79,** 253–263.

Molinari, J., and M. Dudek, 1992: Parameterization of convective

precipitation in mesoscale numerical models: A critical review. *Mon. Wea. Rev.,* **120,** 326–344.

NCDC, 1995: *Storm Data.* Vol. 37, No. 5, National Climatic Data Center, 169–227.

Olson, D. A., N. W. Junker, and B. Korty, 1995: Evaluation of 33 years of quantitative precipitation forecasting at the NMC. *Wea. Forecasting,* **10,** 498–511.

Rasmussen, E. N., J. M. Straka, R. Davies-Jones, C. A. Doswell III, F. H. Carr, M. D. Eilts, and D. R. MacGorman, 1994: Verification of the Origins of Rotation in Tornadoes Experiment: VORTEX. *Bull. Amer. Meteor. Soc.,* **75,** 995–1006.

Rogers, R. R., and M. K. Yau, 1989: *A Short Course in Cloud Physics.* 3d ed. Pergamon Press, 293 pp.

Rotunno, R., J. B. Klemp, and M. L. Weisman, 1988: A theory for strong, long-lived squall lines. *J. Atmos. Sci.,* **45,** 463–485.

Rutledge, S. A., and P. V. Hobbs, 1983: The mesoscale and microscale structure and organization of clouds and precipitation in mid-latitude cyclones. VIII: A model for the ''seeder-feeder'' process in warm-frontal rainbands. *J. Atmos. Sci.,* **40,** 1185–1206.

Skamarock, W. C., M. L. Weisman, and J. B. Klemp, 1994: Three-dimensional evolution of simulated long-lived squall lines. *J. Atmos. Sci.,* **51,** 2563–2584.

Smagorinsky, J., 1963: General circulation experiments with the primitive equations. *Mon. Wea. Rev.,* **91,** 99–165.

Smull, B. F., and R. A. Houze, 1987: Rear inflow in squall lines with trailing stratiform precipitation. *Mon. Wea. Rev.,* **115,** 2869–2889.

Wang, D., M. Xue, V. C. Wong, and K. K. Droegemeier, 1996: Prediction and simulation of convective storms during VORTEX95. Preprints, *11th Conf. on Numerical Weather Prediction,* Norfolk, VA, Amer. Meteor. Soc., 301–303.

Wang, W., and N. L. Seaman, 1997: A comparison study of convective parameterization schemes in a mesoscale model. *Mon. Wea. Rev.,* **125,** 252–278.

Weisman, M. L., J. B. Klemp, and R. Rotunno, 1988: Structure and evolution of numerically simulated squall lines. *J. Atmos. Sci.,* **45,** 1990–2013.

——, W. C. Skamarock, and J. B. Klemp, 1997: The resolution dependence of explicitly modeled convective systems. *Mon. Wea. Rev.,* **125,** 527–548.

Zhang, D.-L., 1989: The effect of parameterized ice microphysics on the simulation of vortex circulation with a mesoscale hydrostatic model. *Tellus,* **41A,** 132–147.

——, and H.-R. Cho, 1992: The development of negative moist potential vorticity in the stratiform region of a simulated squall line. *Mon. Wea. Rev.,* **120,** 1322–1341.

——, E.-Y. Hsie, and M. W. Moncrieff, 1988: A comparison of explicit and implicit predictions of convective and stratiform precipitating weather systems with a meso-β scale numerical model. *Quart. J. Roy. Meteor. Soc.,* **114,** 31–60.

——, K. Gao, and D. B. Parsons, 1989: Numerical simulation of an intense squall line during 10–11 June 1985 PRE-STORM. Part I: Model verification. *Mon. Wea. Rev.,* **117,** 960–994.

——, J. S. Kain, J. M. Fritsch, and K. Gao, 1994: Comments on ''Parameterization of convective precipitation in mesoscale numerical models: A critical review.'' *Mon. Wea. Rev.,* **122,** 2222–2231.